Arabian Journal for Science and Engineering (2019) 44:9939–9950
https://doi.org/10.1007/s13369-019-04177-y

RESEARCH ARTICLE - CHEMICAL ENGINEERING

# New Way of Synthesis of Basic Bismuth Nitrate by Electrodeposition from Ethanol Solution: Characterization and Application for Removal of RB19 from Water

**Slobodan M. Najdanović[1] · Milica M. Petrović[1] · Miloš M. Kostić[1] · Nena D. Velinov[1] · Miljana D. Radović Vučić[1] · Branko Ž. Matović[2] · Aleksandar Lj. Bojić[1]**

Received: 20 March 2019 / Accepted: 19 September 2019 / Published online: 26 September 2019


**Abstract**
A new method of synthesis was developed for the preparation of sorbent basic bismuth nitrate $[Bi_6O_5(OH)_3](NO_3)_5{\cdot}2H_2O$ (BBN-EtOH). This electrochemical method includes electrodeposition from an acidic Bi(III) solution in 96% ethanol at a constant current density of 150.0 mA $cm^{-2}$. Final product was obtained by thermal treatment at 200 °C. Characterization of BBN-EtOH was conducted by employing XRD, FTIR, SEM–EDX as well as BET, and its pI was also determined. The analysis showed that the material obtained is pure $[Bi_6O_5(OH)_3](NO_3)_5{\cdot}2H_2O$. Morphologically, it is composed of aggregates which were formed of several smaller particles of various shapes and sizes, some smaller than 100 nm. Electrochemically synthesized sorbent (BBN-EtOH) was used for the removal of the textile dye Reactive Blue 19 (RB19) from deionized water and model solution of river water, and it showed considerably superior sorption performance compared to other inorganic sorbents synthesized by conventional methods reported in the literature. Kinetic study suggests that the sorption process is both under reaction and diffusion control. Equilibrium of the sorption process was attained in several minutes, i.e., the sorption process is very fast. The sorption equilibrium data were well interpreted by the Langmuir, Sips and Brouers–Sotolongo isotherm. The maximum sorption performance was achieved at pH 2.0, and according to the Langmuir isotherm, it is 1344.99 mg $g^{-1}$.

**Keywords** Electrochemical synthesis · $[Bi_6O_5(OH)_3](NO_3)_5{\cdot}2H_2O$ · Reactive Blue 19 · Water treatment · Kinetic models · Isotherm models

## 1 Introduction

With the development of industries that are extensively using a wide variety of dyes, such as pulp, plastics, tanning, rubber, leather, cosmetics, paper and textile industries, the water pollution caused by toxic dyes is serious threat to humans and the environment [1, 2]. Dyes usually have many structural varieties and based on their chemical structures are classified as azo, anthraquinone, indigo, thiazine, xanthene, triphenylmethane, arylmethane, quinolone, phenanthrene and phthalocyanine [3]. The most commonly used dyes classification system is the Colour Index (CI), developed by the Society of Dyes and Colourist (1924), which lists dyes first by a generic name based on its application and colour and then by assigning a 5-digit CI number based on its chemical structure if known [4, 5]. According to their mode of application, dyes can be classified as reactive, disperse, direct, vat, sulphur, cationic, acid, mordant, basic, metallic, ingrain and solvent dyes [5]. Among different groups of dyes, azo and anthraquinone dyes are the most commonly used [6].

These dyes can be easily lost during the operating process. About 15% of dyes are discharged into wastewater stream upon use in dyeing and finishing [7]. Synthetic dyes

**Electronic supplementary material** The online version of this article (https://doi.org/10.1007/s13369-019-04177-y) contains supplementary material, which is available to authorized users.

✉ Slobodan M. Najdanović
najda89@gmail.com

[1] Department of Chemistry, Faculty of Sciences and Mathematics, University of Niš, Višegradska 33, Niš 18000, Serbia

[2] Materials Science Laboratory, Institute of Nuclear Sciences, University of Belgrade, 170 Vinča, Belgrade, P.O. Box 522, 11001, Serbia

have complex aromatic molecular structures, which make it stable and non-biodegradable. Thus, because of high stability and toxicity their release into the environment causes serious environmental and health problems [8]. Therefore, the dye removal from effluents before being released into natural water is very important.

The conventional treatment methods of dye bearing wastewaters involve the combination of physical and chemical processes such as adsorption, chemical oxidation, ozonization, coagulation, membrane filtration and biological treatment. However, the application of the above-mentioned methods is sometimes restricted due to technical and economic constraints. Adsorption due to its simplicity and high efficiency is one of the most often employed methods for the treatment of wastewater [9]. The current literature suggests that basic bismuth nitrates (BBNs) are used as a photocatalysts [10–12] and, to the best of our knowledge, very rarely as sorbents [13] for the removal of various pollutants.

Synthetic methods for the preparation of basic bismuth nitrates include precipitation [13], hydrothermal [10], microwave-assisted hydrothermal [11] and hydrolysis methods [12] can be find in the literature. Electrochemical synthesis through the electrodeposition is a very convenient method for material synthesis, due to its simplicity, rigid control of film thickness, uniformity and deposition rate, and it is especially attractive due to low cost of equipment and starting materials [14]. Organic electrolytes have been usually used to realize a wide electrochemical window, avoid hydrogen embrittlement, improve the wettability of the electrode and improve anti-wear performance of deposit [15]. Synthesis of basic bismuth nitrates by any electrochemical method has not yet been published in the literature.

The aim of this study was the synthesis of basic bismuth nitrate via electrodeposition method from ethanol solution with further thermal treatment. Characterization of material was performed by X-ray diffraction (XRD), Fourier-transform infrared spectroscopy (FTIR), scanning electron microscopy (SEM), energy-dispersive X-ray spectroscopy (EDX) and $N_2$ sorptometry analysis. The synthesized material was applied as sorbent for the removal of textile dye Reactive Blue 19 (RB19), which was used as a model pollutant. In order to understand sorption process, several reaction and diffusion kinetic models were applied, as well as isotherm models.

## 2 Experimental Methods

### 2.1 Reagents

All chemicals were of analytical reagent grade and used without further purification. Reactive Blue 19 (type: anthraquinone dye, molecular formula: $C_{22}H_{16}N_2Na_2O_{11}S_3$, molecular weight: 626.53 g $mol^{-1}$, maximum absorbance: 592 nm, CAS number: 2580-78-1, colour index number: 61200) was supplied from Sigma-Aldrich (Germany). Prior to use, 1.0000 g of dye was dissolved in 1000 $cm^3$ of water to obtain a 1000 mg $dm^{-3}$ stock solution of dye. Nitric acid, sodium hydroxide and ethanol were also obtained from Sigma-Aldrich. Bismuth (III) nitrate pentahydrate used for synthesis of basic bismuth nitrate was obtained from Acros Organics (USA). All solutions were prepared with deionized water.

### 2.2 Synthesis of Basic Bismuth Nitrate from Ethanol Solution

All electrochemical experiments were performed using an Amel 510 DC potentiostat (Materials Mates, Italy) controlled by a VoltaScope software package. Electrodeposition was performed in the two-electrode cell with a Ti sheet (10 × 20 mm) as a substrate (cathode) and a stainless steel sheet (10 × 20 mm) as an auxiliary electrode (anode). The distance between the working and auxiliary electrode was 15 mm. Before the deposition, all electrodes were polished with different abrasive papers, followed by ultrasonic cleaning with ethanol and deionized water. A bismuth (III) electrodeposition solution of 0.1 mol $dm^{-3}$ was prepared by dissolving the required amount of bismuth nitrate in 1.0 mol $dm^{-3}$ $HNO_3$ in 96% ethanol. Electrodeposition was carried out at a constant current density of 150 mA $cm^{-2}$ for 300 s at 25.0 ± 0.5 °C. After deposition, the Ti sheet, covered with deposited coating, was dried at room temperature for 120 min, calcined at 200 °C for 90 min in a furnace in air and cooled in air. Then, the synthesized basic bismuth nitrate was removed from the Ti sheet, powdered and used as a sorbent.

### 2.3 Characterization of Sorbent

For SEM–EDX analysis, samples were attached to aluminium stubs using Agar carbon tabs. A JEOL5310LV (JEOL, USA) was used for imaging the samples in low vacuum mode with an Oxford Instruments X-Max 50 detector for semi-quantitative EDX analysis. Samples were imaged uncoated. Nominal magnifications from 2000× to 70,000× were used when imaging the samples. Three random particles averaged for EDX analysis. FTIR spectra were recorded by means of BOMEM MB-100 FTIR spectrometer (Hartmann & Braun, Canada) using KBr pellets containing 1.0 mg of the sample in 150 mg KBr. Instrument is equipped with a standard DTGS/KBr detector in the range of 4000–400 $cm^{-1}$ with a resolution of 2 $cm^{-1}$. The number of scans was 16. Crystal structure was analyzed by XRD using filtered Cu Kα radiation (Ultima IV, Rigaku, Japan). The experiments were performed in the scan range $2\theta = 5°$–$90°$ under 40 kV,

40 mA, with scan speed 5° $min^{-1}$ and steps with 0.02°. Before measurement, the angular correction was done by high quality Si standard. Lattice parameters were refined from the data using the least square procedure. Standard deviation was about 1%. The specific surface area was measured by a nitrogen adsorption using the Gemini 5 Surface Area Analyzer (Micromeritics, Norcross, Georgia, USA). Samples were degassed under flowing nitrogen at 40 °C for 20 h before the measurement. The specific surface area was determined using the Brunauer–Emmett–Teller (BET) method [16]. The Barret–Joyner–Halenda (BJH) method was used for pore volume, area and diameter analysis [17]. The isoelectric point of the sorbent was determined by the salt addition method [18].

### 2.4 Batch Sorption Experiments

The sorption capacity of the prepared sorbent was determined by the removal of RB19 from aqueous solution at ambient temperature. All sorption experiments were conducted at native pH 4.7 ± 0.1 (initial pH of dye solution without adjustments), except in cases when the effect of pH on the removal of RB19 was determined. An appropriate amount of sorbent was added to dye solution, and the solution was transferred to a Petri dish. During the sorption experiments, the dye solutions were stirred using a magnetic stirrer. At given time intervals, samples were collected, centrifuged and filtered using a 0.45-μm regenerated cellulose membrane filter (Agilent Technologies, Germany) to remove the particles of sorbent. The concentration of RB19 was measured by measuring the absorbance at 592 nm using a UV–visible spectrophotometer (UV-1800, Shimadzu, Japan). The sorbed amount of RB19, $q_t$, (mg $g^{-1}$) and the removal efficiency, RE (%), were calculated by Eqs. 1 and 2, respectively:

$$q_t = \frac{c_0 - c_t}{m} \cdot V \tag{1}$$

$$\mathrm{RE}(\%) = \frac{c_0 - c_t}{c_0} \cdot 100 \tag{2}$$

where $c_0$ and $c_t$ are the initial and final concentrations of the RB19 (mg $dm^{-3}$), $V$ is the solution volume ($dm^3$) and $m$ is the mass of the sorbent (g).

The mean relative deviation (MRD) was calculated by Eq. 3:

$$\mathrm{MRD}(\%) = \frac{\sum_{i=1}^{n} \left| q_{i,\mathrm{exp}} - q_{i,\mathrm{cal}} \right|}{\overline{q_{\mathrm{exp}}} \cdot n} \cdot 100 \tag{3}$$

where $q_{i,\,\mathrm{exp}}$ (mg $g^{-1}$) is the experimentally obtained amount of sorbed dye at experimental point $i$, $q_{i,\,\mathrm{cal}}$ (mg $g^{-1}$) is calculated amount of sorbed dye at experimental point $i$ by some kinetic or isotherm model and $n$ is number of experimental points.

Control experiments were carried out in the absence of sorbent in order to find out whether there is any adsorption on the Petri dish walls. In all experiments, measurements of the RB19 concentrations were conducted in triplicate. Statistical analysis and calculation of the data were performed using OriginPro 2016 software (OriginLab Corporation, USA).

### 2.5 Kinetic and Isotherm Analysis

Sorption kinetics is important to illustrate the process mechanism. Different kinetic models have been used to investigate the potential rate-controlling steps involved in the sorption process. In this study, the experimental data were analyzed by pseudo-first-order [19], pseudo-second-order [20], Chrastil's [21] and intraparticle diffusion [22] kinetic models and the equations of these models are presented in Eqs. 4, 5, 6 and 7, respectively:

$$q_t = q_{\mathrm{e}}(1 - \mathrm{e}^{-k_1 t}) \tag{4}$$

$$q_t = \frac{q_{\mathrm{e}}^2 k_2 t}{1 + k_2 q_{\mathrm{e}} t} \tag{5}$$

$$q_t = q_{\mathrm{e}}\left(1 - \mathrm{e}^{-k_C A_0 t}\right)^n \tag{6}$$

$$q_t = k_{id} t^{1/2} + C \tag{7}$$

where $q_{\mathrm{e}}$ and $q_t$ are the sorption capacity at equilibrium and at time $t$, respectively (mg $g^{-1}$).

In the pseudo-first- and pseudo-second-order model, $k_1$ (g $min^{-1}$) and $k_2$ (g $mg^{-1}$ $min^{-1}$) are the rate constant of pseudo-first- and pseudo-second-order adsorption, respectively.

In the Chrastil's diffusion model, $k_c$ is a rate constant ($dm^3$ $g^{-1}$ $min^{-1}$), $A_0$ is the concentration of sorbent (g $dm^{-3}$) and $n$ is a heterogeneous structural diffusion resistance constant with reaction order characteristics. Reaction order and diffusion characteristics of the sorption process can be determined from the value of constant $n$. For diffusion-limited systems, $n$ is lower than 1, and in the case when diffusion resistance is small $n \geq 1$. For the first-order reactions, $n = 1$, second- and higher-order reactions have $n < 1$, and consecutive reactions have $n > 1$ [23].

In the intraparticle diffusion model, $C$ value is related to the thickness of the boundary layer and $k_{id}$ is the intraparticle diffusion rate constant (mg $g^{-1}$ $min^{1/2}$).

The adsorption capacity of adsorbent and interaction mode between adsorbent with adsorbent is another critical

factor for the practical use of the adsorbent. Thus, the experimental equilibrium data of RB19 sorption were modelled using several equilibrium adsorption isotherm models, such as Langmuir [24], Freundlich [25], Sips [26] and Brouers–Sotolongo [27, 28]. The Langmuir model is used successfully in many monolayer sorption processes without interaction between adsorbate molecules, and assumes that sorption occurs on specific homogenous sites of sorbents. The Freundlich isotherm model proposes a multilayer sorption with a heterogeneous energetic distribution of active sites, accompanied by interactions between adsorbed molecules. Sips model inherently includes the features of Freundlich and Langmuir models and has more capability in describing sorption equilibrium. Sips model predicts the heterogeneous sorption and circumventing the limitation of the rising sorbate concentration associated with the Freundlich isotherm model. Brouers–Sotolongo model proposes adsorption at heterogeneous surface. Equations 8, 9, 10 and 11 give nonlinear forms of the Langmuir, Freundlich, Sips and Brouers–Sotolongo models, respectively:

$$q_e = \frac{q_m K_L c_e}{1 + K_L c_e} \tag{8}$$

$$q_e = K_F c_e^{\frac{1}{n}} \tag{9}$$

$$q_e = \frac{q_m K_S C_e^{1/n}}{1 + K_S C_e^{1/n}} \tag{10}$$

$$q_e = q_m \left(1 - \exp\left(-K_W c_e^{\alpha}\right)\right) \tag{11}$$

where $q_e$ is the amount of sorbed RB19 (mg $g^{-1}$) at equilibrium time, $c_e$ is the concentration (mg $dm^{-3}$) of RB19 at equilibrium time, $q_m$ is the maximum sorption capacity of sorbent (mg $g^{-1}$); $K_L$ is Langmuir constant related to the energy of sorption ($dm^3$ $mg^{-1}$), $K_F$ is Freundlich equilibrium constant (mg $g^{-1}$) ($dm^3$ $mg^{-1})^{1/n}$, $n$ is Freundlich exponent related to the intensity of sorption, $K_S$ the Sips equilibrium constant ($dm^3$ $mg^{-1}$), $n$ is the Sips model exponent related to heterogeneity of binding sites, $K_W$ is Brouers–Sotolongo isotherm constant ($dm^3$ $mg^{-1}$) and $\alpha$ is dimensionless exponent and measure of the energy heterogeneity of the surface.

## 3 Results and Discussion

### 3.1 Mechanism of Electrochemical Synthesis and Characterization of Sorbent

Electrochemical synthesis is based on cathodic electrodeposition from acidic solution of $Bi^{3+}$ ions and further thermal treatment at 200 °C. Electrodeposition was performed in galvanostatic mode at current density of 150 mA $cm^{-2}$. At such high current density, overpotential of hydrogen is achieved and besides bismuth, hydrogen generates on the cathode as well. Hydrogen bubbles produced on the cathode affect the creation of a sponge-like structure of deposit. It is more likely that deposit is physically bonded to the surface of the cathode, rather than constructing a chemical bond with it, and this deposit is generally mechanically unstable and can be easily removed from the surface of the metal substrate. Characterization of obtained deposit was carried out by XRD analysis, but the deposit contains some amorphous phase, so it is impossible to accurately determine all individual phases. EDX analysis (Fig. S1 in Supplementary material) shows that deposit contains Bi, O and N atoms, and thus, it can be concluded that it is composed of metallic bismuth and bismuth in oxidized form (most likely bismuth compounds such as basic nitrates, and possibly hydroxides and oxides). The cause of the production of oxidized form on the cathode is probably the simultaneous reduction in $H^+$ and $Bi^{3+}$ ions, where the local pH near the cathode increases significantly and the hydrolysis of non-reduced $Bi^{3+}$ ions in the presence of $NO_3^-$ ions occurs, resulting in formation of above-mentioned bismuth compounds [14]. After thermal treatment at 200 °C, all metallic Bi was oxidized to basic bismuth nitrate. Oxidation to nitrate was enabled because of specific sponge-like structure of deposit, which contains a $NO_3^-$ ions-containing electrolyte.

The crystal structure of the product obtained after thermal treatment at 200 °C, and later used as a sorbent, was also examined by XRD analysis. Figure 1 shows the typical XRD pattern of the synthesized sample. The main diffraction peak positions of product in this pattern appear at 11.64°, 13.08°, 20.28°, 23.49°, 26.92°, 34.02°, 41.24° and 52.59° $2\theta$ values. The diffraction peaks can be indexed to the to the trigonal (space group P-3) $[Bi_6O_5(OH)_3](NO_3)_5{\cdot}2H_2O$ (JCPDS-ICDD: PDF-2 00-054-0627), with lattice constants of $a = b = 15.187$ Å and $c = 15.838$ Å. In addition, there is no other impurity peak was detected, indicating the formation of clean $[Bi_6O_5(OH)_3](NO_3)_5{\cdot}2H_2O$ composites without the disturbance of impurity. The sharp shape and high-intensity peaks suggest that the crystalline degree of sample is high. The crystallite size of material was determined by Williamson–Hall method, and the results show that crystallites have nanometric size (16.58 nm) [29].

The FTIR spectra of the prepared material are given in Fig. 2. The broadband at 3408 $cm^{-1}$ corresponds to the stretching vibrations of –OH groups and indicates that the –OH groups participate in the formation of hydrogen bonds in BBN-EtOH [30]. The bands at 1623 $cm^{-1}$ originate from the –OH bending vibration mode of lattice water [31, 32]. Several IR active modes arising from the $NO_3^-$ vibrations are observed at IR frequencies at 702, 809, 824, 1035 and 1383 $cm^{-1}$ and fit well to the data for $BiMO_2NO_3$,

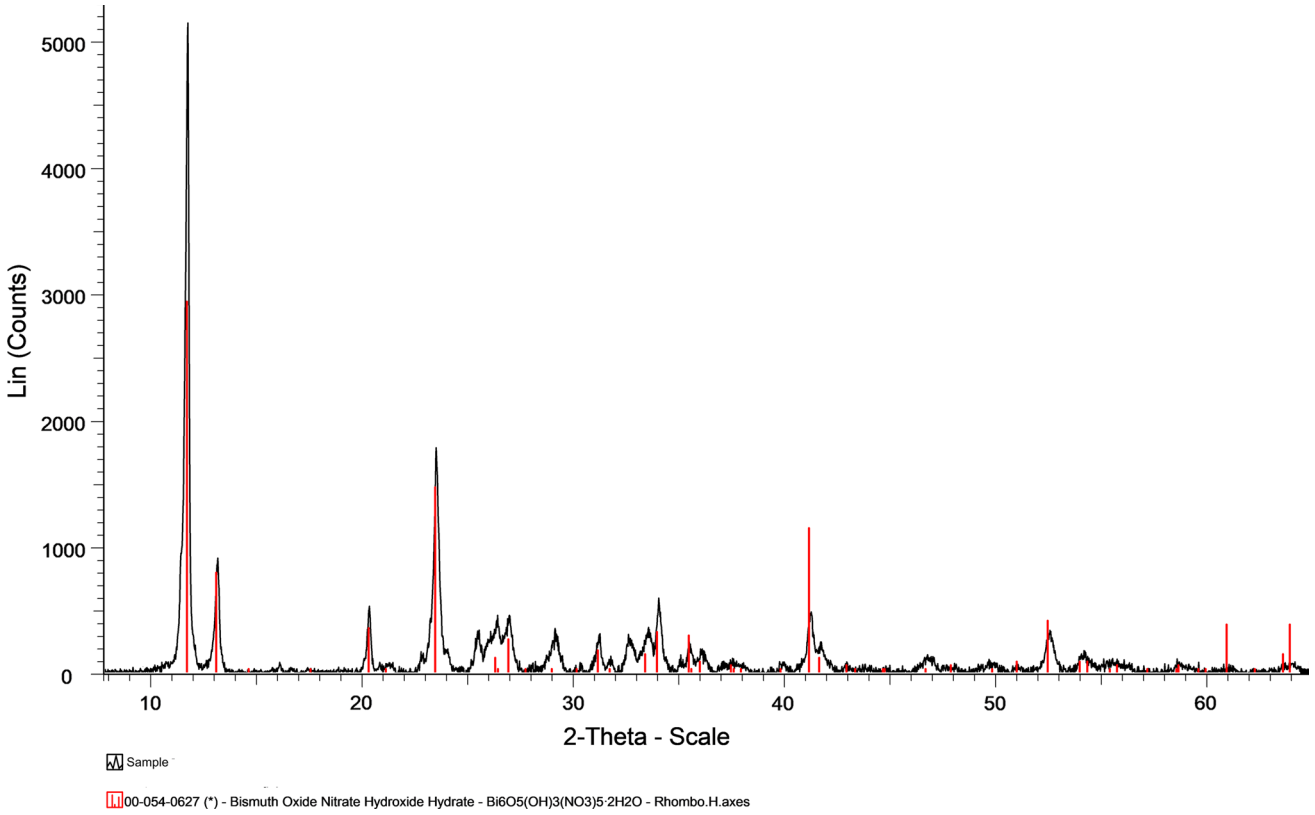


**Fig. 1** XRD pattern of BBN-EtOH

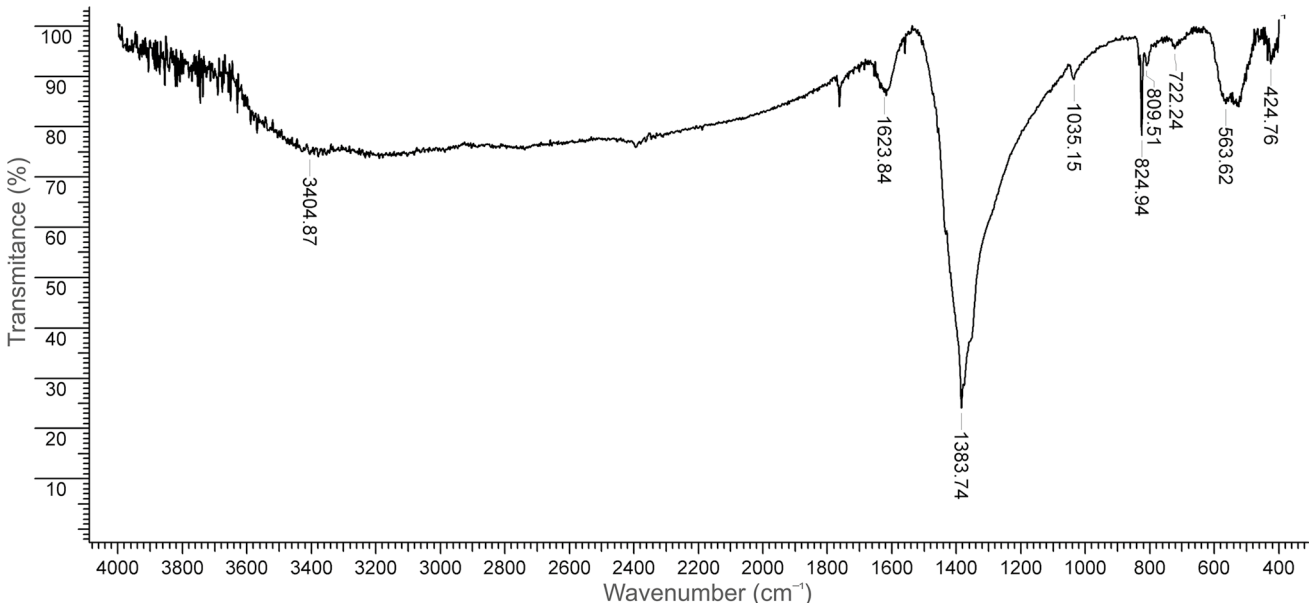


**Fig. 2** FTIR spectrum of BBN-EtOH

$K_3Pr_2(NO_3)_9$, and for nitrate groups in anhydrous lanthanide nitrates and oxynitrates [33–35]. According to Carnall et al., the fine structure of the lower frequency bands at 1297, 803 and 736 $cm^{-1}$ is very sensitive to the dryness of the nitrates and disappears upon hydration [34]. It follows that the absence of these IR bands confirms a hydrated form

of the synthesized compound. The medium strong bands at 563 and 424 $cm^{-1}$ are attributed to the Bi–O bond stretching vibrations [36, 37].

Morphology and surface structure of the synthesized material were investigated by SEM analysis. The SEM images at different magnifications are presented in Fig. 3. As shown in Fig. 3a, it could be clearly seen that the BBN-EtOH sample is constructed from a large amount of irregular monolithic aggregates of a micron-level size. All the aggregates are consisted from particles that are mostly sintered and have various sizes and shapes. Most of the particles are basically polyhedrons whose size is 200–1000 nm. The surface of the particles is smooth, and some particles with nanometric size can be spotted. In addition, pores with diameter lower than 50 nm can be observed on the sample surface.

The results of EDX analysis (Fig. S2) showed that material is composed of Bi, O and N. The weight percentages of these elements are 71.01%, 24.60% and 4.19%, respectively. Theoretical weight percentages of Bi, O and N in $[Bi_6O_5(OH)_3](NO_3)_5{\cdot}2H_2O$ are 72.43%, 23.11% and 4.04%, respectively, and it is in good agreement with the experimental one.

The sorption process mainly occurs at the surface of the sorbent and because of that the specific surface area (SSA) has a significant influence on the sorption performance. With the increase in SSA, the number of active sites is higher and sorption performance is enhanced. The $N_2$ adsorption/desorption isotherm of BBN-EtOH (Fig. 4) according to the IUPAC classification belongs to type II, which is related to nonporous or macroporous adsorbents and unrestricted monolayer–multilayer adsorption. The obtained SSA of BBN-EtOH using the BET method is 1.43 $m^2\ g^{-1}$. The BJH surface area of pores is 1.09 $m^2\ g^{-1}$, and the volume of pores is 0.0036 $cm^3\ g^{-1}$. The average pore diameter is 13.19 nm.

In order to define how surface charge changes depending on the pH of medium, the isoelectric point of synthesized material was determined by salt addition method. The obtained value of pI for BBN-EtOH is 2.09, which means that its surface is acidic. In case when the pH of solution is lower than 2.09, material surface will be positive, while for pH higher than 2.09 surface will be negative charged.

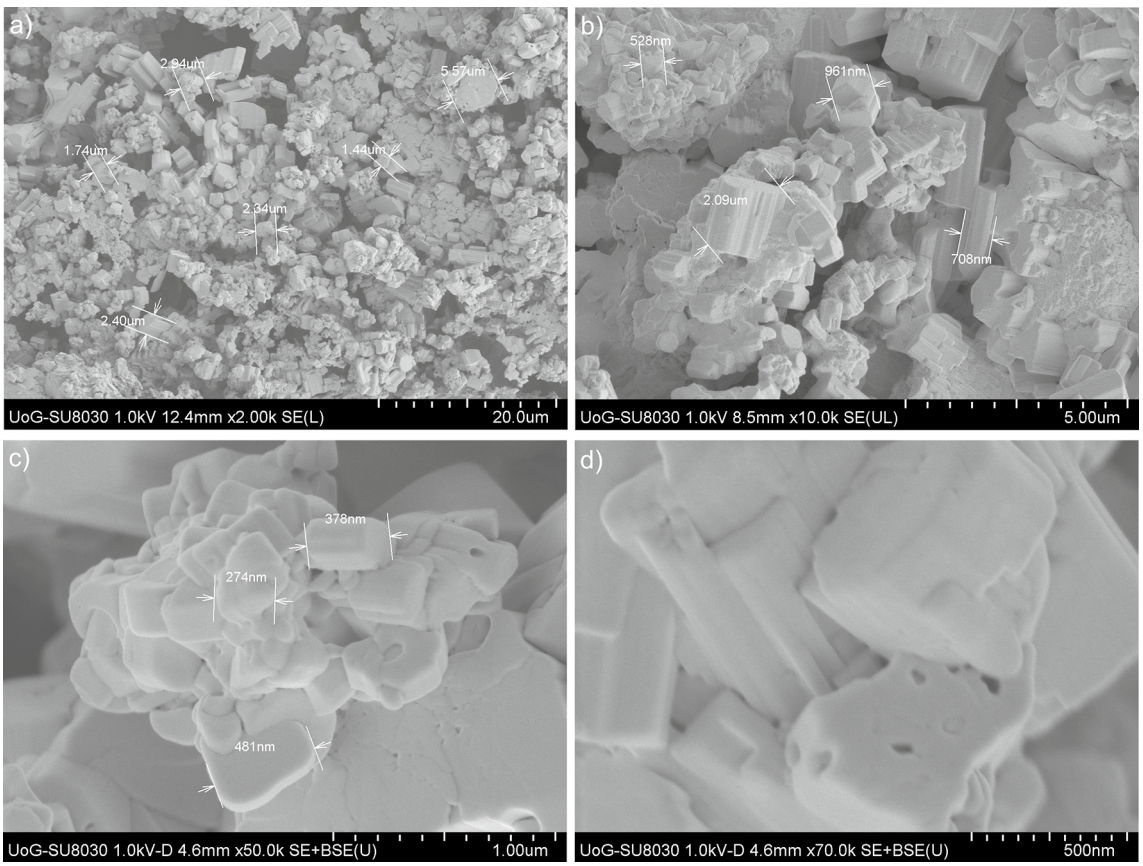


**Fig. 3** SEM images of BBN-EtOH at a magnifications of **a** ×2000, **b** ×10000, **c** ×50000 and **d** ×70000

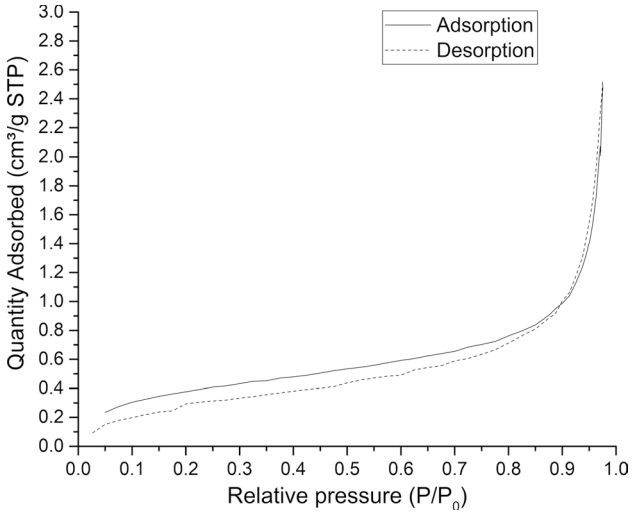


**Fig. 4** $N_2$ adsorption/desorption isotherm of BBN-EtOH

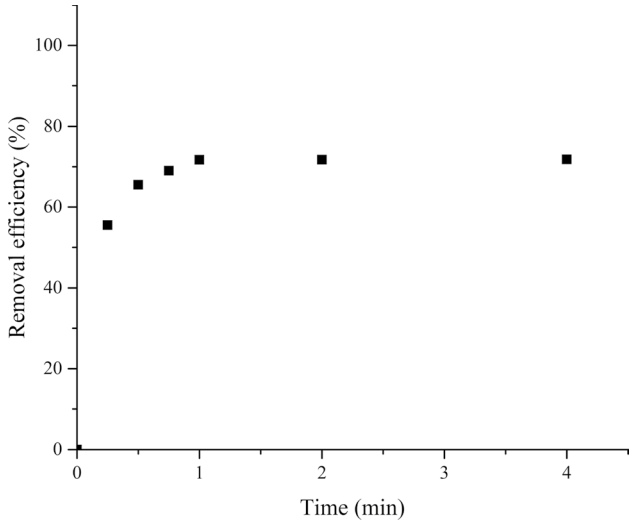


**Fig. 5** Effect of contact time on the removal efficiency of RB19. $c_{RB19}$ 700.0 mg dm$^{-3}$, $c_{sorbent}$ 500.0 mg dm$^{-3}$, temperature 25.0 ± 0.5 °C and pH native

## 3.2 Ability of BBN-EtOH to Remove RB19

### 3.2.1 Effect of Contact Time on the Removal Efficiency of RB19

The contact time is a crucial parameter to be considered as it can determine the possible practical application of sorbent. Longer time taken to remove the dye is not practical for treatment of real wastewater and increases the cost of the whole sorption process. For these reasons, it is very important that the sorption equilibrium be achieved in a relatively short time.

The effect of contact time for RB19 adsorption onto BBN-EtOH was investigated at native pH (about 4.7), with sorbent dose 500.0 mg dm$^{-3}$, RB19 concentration of 700.0 mg dm$^{-3}$ and temperature 25.0 °C. The results are shown in Fig. 5. The obtained removal efficiency was 71.80%, which is a very high value considering the fact that the initial concentration of RB19 was 700.0 mg dm$^{-3}$. The removal efficiency of RB19 increased rapidly in the first minute and after that sorption was almost negligible. In the first minute, 95% of the total amount of dye that was sorbed during the entire sorption process was removed. In the next period of time, until the equilibrium was reached, only 5% from the total removed amount was sorbed. Further extending, the contact time did not improve the adsorption potential of BBN-EtOH for RB19. This means that sorption equilibrium was reached extremely fast (1–2 min). According to the results from the literature for similar inorganic sorbents, the sorption process of removing the RB19 with BBN-EtOH is far faster [38–45]. One of the most important characteristics of material synthesized from ethanol solution that affect such a high sorption ability of the material is its high hydrophilicity, i.e., the tendency of getting solvated by water. Material is well wetted and does not float in water, and it can be assumed that this is one of the main reasons for high sorption performance of material.

### 3.2.2 Effect of pH on the Removal Efficiency of RB19

The medium pH is a critical parameter in every sorption system. It strongly affects the surface charge of sorbent and the degree of ionization and the speciation of sorbates (e.g., dye, metal) [46].

The effect of pH was investigated in a pH range from 2.0 to 9.0, while other parameters were kept constant (initial concentration of dye 700.0 mg dm$^{-3}$, sorbent dose 500.0 mg dm$^{-3}$ and temperature 25.0 °C). The results (Fig. 6) show that pH strongly affects the removal efficiency of RB19. The highest removal efficiency (93.33%) was achieved at pH 2.0, while by increasing the pH value to 3.0, 5.0, 7.0 and 9.0, the removal efficiency decreased to 78.87%, 71.69%, 65.88% and 56.81%, respectively. Such an effect of pH on the sorption process can be explained by surface charge of sorbent at different pH solutions. Surface of BBN-EtOH sorbent is positively charged at pH < 2.09 according to its pI value. Thus, sorption of anionic dye RB19 is enhanced at lower pH. With the increase in solution pH, surface charge of sorbent is increasingly negative and the removal of RB19 decreases. The obtained sorption capacity of BBN-EtOH at pH 2.0, 3.0, 5.0, 7.0 and 9.0 is 1306.64, 1150.00, 1003.66, 922.38 and 795.3 mg dm$^{-3}$, respectively. These results show that BBN-EtOH is efficient as sorbent for RB19 in wide range of pH. Even the lowest value of sorption capacity 795.30 mg dm$^{-3}$ achieved at pH 9.0 is very high compared to other inorganic sorbents reported in the

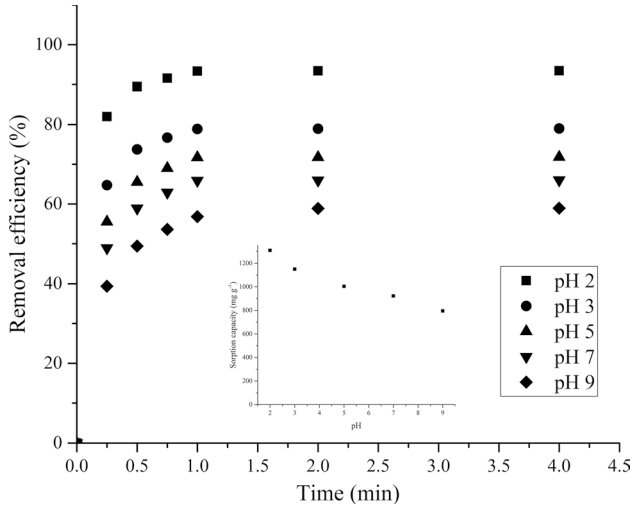


**Fig. 6** Effect of pH on the removal efficiency of RB19; $c_{RB19}$ 700.0 mg dm$^{-3}$, $c_{sorbent}$ 500.0 mg dm$^{-3}$ and temperature 25.0 ± 0.5 °C

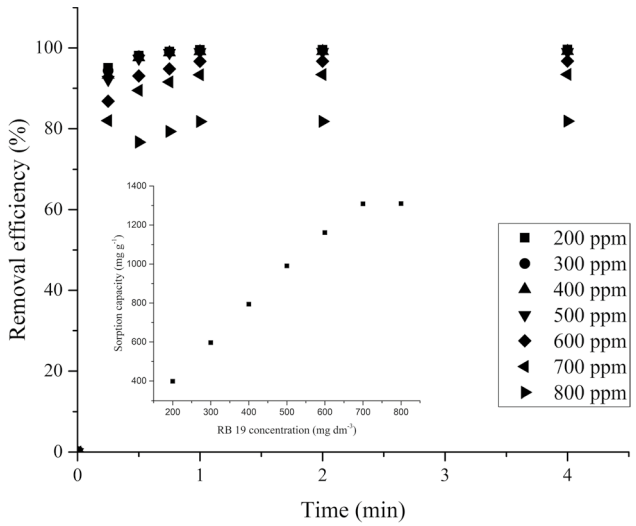


**Fig. 7** Effect of initial concentration of dye on the removal efficiency of RB19; $c_{sorbent}$ 500.0 mg dm$^{-3}$, temperature 25.0 ± 0.5 °C and pH 2.0

literature (maximum sorption capacity achieved for FeCuNi-triple-metal nanosorbent was 480.80 mg dm$^{-3}$, while for organic sorbents maximum capacity was 822.40 mg dm$^{-3}$ for chitosan) [38–45].

### 3.2.3 Effect of Initial Dye Concentration on Removal Efficiency of RB19

The effects of initial dye concentration were investigated for 200.0, 400.0, 500.0, 600.0, 700.0 and 800.0 mg dm$^{-3}$, while other conditions were kept constant (pH 2.0, sorbent dose 500.0 mg dm$^{-3}$ and temperature 25.0 °C). The results are presented in Fig. 7. In the case of lower initial concentrations of RB19 (200–500 mg dm$^{-3}$), the removal efficiency was very high (99.60%, 99.45%, 99.21% and 99.01%, respectively). With further increase in initial pollutant concentration, the removal efficiency decreases up to 81.85% for initial RB19 concentration of 800.0 mg dm$^{-3}$.

However, the sorption capacity of BBN-EtOH increases with an increase in initial RB19 concentration and reached 1309.60 mg g$^{-1}$ for initial RB19 concentration of 800.0 mg dm$^{-3}$. This can be attributed to the fact that the higher RB19 concentrations increase the overall mass transfer driving force, and thus, the RB19 uptakes onto the sorbent [46].

### 3.2.4 Kinetics Study

Adsorption processes could be dependent on and controlled by different kinds of mechanisms such as diffusion control, mass transfer, chemical reactions and particle diffusion. Thus, the kinetics of RB19 sorption onto BBN-EtOH sorbent was described by the pseudo-first-order, pseudo-second-order, Chrastil's diffusion and intraparticle diffusion model. The plots of $q_t$ versus $t$ for all kinetic models are shown in Fig. S3-5. The obtained parameters of kinetic models for the sorption process for different initial RB19 concentrations are shown in Table 1. All the parameters were calculated by nonlinear regression analysis using software OriginPro 2016 (except for intraparticle diffusion model where was used linear regression analysis). Applicability of these models on the sorption of RB19 on BBN-EtOH sorbent was determined based on the values of the determination coefficients and the mean relative deviations.

The fitting results of experimental data for pseudo-first- and pseudo-second-order models show that both models have very high determination coefficients (higher than 0.999), but determination coefficient for pseudo-second order is slightly higher. Calculated values of $q_e$ are in good agreement with experimental results for both models, but the results obtained for pseudo-first model a bit better matched the experimental ones. However, based on obtained values of MRD it is obvious that pseudo-second-order model better fits with the experimental results (values of MRD is significantly lower for pseudo-second order). Therefore, it can be concluded that pseudo-second-order model better describes this sorption process. This suggests that the saturation rate of binding sites is proportional to the squared amount of unsaturated sites [20]. In addition, the rate-controlling step in the sorption process is most likely the chemical interaction between functional groups of sorbent BBN-EtOH and RB19. The rate constant decreases from 0.45 to 0.02 as RB19 concentration increases from 200 to 800 mg dm$^{-3}$.

The Chrastil's diffusion model is used for description of the kinetics of the heterogeneous and diffusion-limited

**Table 1** Kinetic parameters for RB19 sorption onto BBN-EtOH sorbent

| $c$ (mg dm$^{-3}$) | 200.0 | 300.0 | 400.0 | 500.0 | 600.0 | 700.0 | 800.0 |
|---|---|---|---|---|---|---|---|
| $q_{e,\,exp}$ (mg g$^{-1}$) | 398.40 | 596.70 | 793.68 | 990.14 | 1161.01 | 1308.34 | 1309.62 |
| *Pseudo-first-order model* | | | | | | | |
| $q_e$ (mg g$^{-1}$) | 396.47 | 594.08 | 790.42 | 986.97 | 1147.55 | 1293.65 | 1291.62 |
| $k_1$ (min$^{-1}$) | 12.72 | 12.19 | 11.49 | 10.77 | 9.38 | 8.58 | 7.11 |
| $r^2$ | 0.9998 | 0.9999 | 0.9999 | 0.9998 | 0.9990 | 0.9991 | 0.9984 |
| MRD (%) | 0.30 | 0.27 | 0.29 | 0.31 | 0.87 | 0.86 | 1.19 |
| *Pseudo-second-order model* | | | | | | | |
| $q_e$ (mg g$^{-1}$) | 402.92 | 604.74 | 807.00 | 1011.36 | 1190.44 | 1350.97 | 1372.78 |
| $k_2$ (g mg$^{-1}$ min$^{-1}$) | 0.17 | 0.10 | 0.06 | 0.04 | 0.02 | 0.02 | 0.01 |
| $r^2$ | 0.9999 | 0.9999 | 0.9998 | 0.9997 | 0.9998 | 0.9996 | 0.9991 |
| MRD (%) | 0.21 | 0.22 | 0.24 | 0.25 | 0.39 | 0.58 | 0.84 |
| *Chrastil's diffusion model* | | | | | | | |
| $q_e$ (mg g$^{-1}$) | 398.46 | 596.59 | 793.72 | 991.16 | 1162.70 | 1309.80 | 1312.67 |
| $k_c$ (dm$^3$ g$^{-1}$ min$^{-1}$) | 10.59 | 10.05 | 9.27 | 7.84 | 7.24 | 6.89 | 6.44 |
| $n$ | 0.10 | 0.14 | 0.18 | 0.19 | 0.23 | 0.25 | 0.35 |
| $r^2$ | 0.9999 | 0.9999 | 0.9999 | 0.9999 | 0.9999 | 0.9999 | 0.9998 |
| MRD (%) | 0.04 | 0.01 | 0.03 | 0.04 | 0.21 | 0.19 | 0.32 |
| *Intraparticle diffusion model* | | | | | | | |
| $k_{i1}$ (mg g$^{-1}$ min$^{-1/2}$) | 592.81 | 887.17 | 1176.44 | 1462.77 | 1672.38 | 1868.63 | 1815.45 |
| $C_1$ (mg g$^{-1}$) | 19.00 | 27.80 | 35.85 | 43.04 | 46.56 | 48.38 | 49.80 |
| $r^2$ | 0.9060 | 0.9115 | 0.9181 | 0.9158 | 0.9172 | 0.9204 | 0.9350 |
| $k_{i2}$ (mg g$^{-1}$ min$^{-1/2}$) | 1.32 | 1.80 | 1.90 | 2.35 | 14.00 | 15.88 | 24.45 |
| $C_2$ (mg g$^{-1}$) | 395.99 | 593.40 | 790.19 | 987.85 | 1136.26 | 1280.19 | 1366.47 |
| $r^2$ | 0.9288 | 0.9379 | 0.9354 | 0.9346 | 0.9481 | 0.9410 | 0.9408 |

systems [21]. The determination coefficient of Chrastil's model is higher than 0.999 for all dye concentrations. The value of MRD is lower than the value obtained for pseudo-second order. This indicates that the Chrastil's model can be used to describe this sorption process. Heterogeneous structural diffusion resistance constant $n$ is for all concentration of RB19 significantly less than one. According to the value of parameter $n$, it can be concluded that sorption follows pseudo-second order, and that the diffusion strongly influences the sorption process.

The kinetic data were also analyzed by the intraparticle diffusion model to examine the rate-controlling step for RB19 sorption on BBN-EtOH sorbent, and the results are presented in Table 1. The two linear ranges in the shape of the intraparticle diffusion plot of $q_t$ versus $t^{1/2}$ indicate that two steps occur in the adsorption process. The first, sharp linear range can be attributed to the external surface adsorption or instantaneous adsorption stage of RB19 on sorbent. When the adsorption onto the external surface reached saturation, the second linear range began, which represents the gradual adsorption stage, where the intraparticle diffusion is rate controlled [47]. The first step is very fast and finishes in about one minute, while the second step is very slow, and after one minute sorbed amount was changed negligible. The intraparticle diffusion rate constant $k_{i2}$ is much lower than $k_{i1}$, which confirms that the rate-limiting step is intraparticle diffusion through boundary layer. The intraparticle model shows that the sorption process ends quickly (very small slope of the second linear part which starts after one minute) and proves enormous rate of sorption process with mixed control by a surface reactions and diffusion.

### 3.2.5 Adsorption Isotherms

It is essential to determine the best-fit isotherm model for the sorption process to obtain useful information about surface properties and affinity of sorbent and enable prediction of maximum sorption capacity. The equilibrium adsorption isotherm models such as Langmuir, Freundlich, Sips and Brouers–Sotolongo isotherms were used to fit the experimental data for different initial RB19 concentrations (200–800 mg dm$^{-3}$), while other parameters were keep constant (pH 2.0, sorbent dose 500.0 mg dm$^{-3}$ and temperature 25.0 °C). The plots of $q_t$ versus residual concentration of dye for all isotherm models are shown in Fig. S6. The nonlinear regressed parameters of these models the corresponding determination coefficients and mean relative deviations are summarized in Table 2.

The values of $r^2$ and MRD were used to evaluate the applicability of the applied models. The results clearly show

**Table 2** Isotherm parameters for RB19 sorption onto BBN-EtOH sorbent

| Adsorption isotherm | Parameter | Values | $r^2$ | MRD (%) |
|---|---|---|---|---|
| Langmuir | $K_L$ | 0.42 | 0.9901 | 3.43 |
| | $q_m$ | 1344.99 | | |
| Freundlich | $K_F$ | 550.32 | 0.7758 | 18.44 |
| | $n$ | 4.97 | | |
| Sips | $q_m$ | 1318.96 | 0.9906 | 3.15 |
| | $K_S$ | 0.44 | | |
| | $n$ | 1.12 | | |
| Brouers–Sotolongo | $q_m$ | 1268.03 | 0.9830 | 4.17 |
| | $K_W$ | 0.35 | | |
| | $\alpha$ | 0.92 | | |

that Langmuir model much better fit experimental data than Freundlich model, with $r^2$ closest to unity (0.99), while $r^2$ for Freundlich model is much less than one (0.75), and much lower MRD (3.43, than 18.44 for Freundlich). This suggests that there was homogeneous distribution of active sites on BBN-EtOH sorbent and that monolayer sorption of RB19 occurred on these sites.

The other two isotherm models (Sips and Brouers–Sotolongo) that were applied for fitting the experimental data also, like Langmuir model, have high determination coefficient (0.99 and 0.98, respectively). According to MRD value, Sips model best fits with experimental data (MRD value for Sips model is slightly lower than Langmuir and Brouers–Sotolongo MRD value). In addition, maximum sorption capacity calculated by Sips model is in the best agreement with experimental value among these models. Based on all the obtained results, it can be concluded that Langmuir, Sips and Brouers–Sotolongo isotherm models are appropriate to describe sorption of RB19 on BBN-EtOH sorbent, and agreement with experimental data is Sips > Langmuir > Brouers–Sotolongo.

The Sips heterogeneity factor $n$ is close to one, which means that sorbent has homogenous binding sites at its surface. The Brouers–Sotolongo parameter α which is related with degree of surfaces heterogeneous is also close to one and indicates that sorption sites of BBN-EtOH sorbent are homogenous. These results confirm that sorption follows Langmuir type of isotherm and the maximal sorption capacity obtained by Langmuir isotherm is 1344.99 mg $g^{-1}$.

### 3.2.6 Mechanism of Sorption Process

According to all the results described earlier in the manuscript, a possible mechanism of RB19 sorption on BBN-EtOH sorbent can be concluded. From the kinetic study, the conclusion is drawn that the rate-controlling step in the sorption process is most likely chemical interaction between functional groups of dye RB19 and sorbent BBN-EtOH. Considering that sorption process occurs between the anionic dye molecules and the surface of the basic bismuth nitrate sorbent, it can be concluded that the most possible mechanism of sorption is interaction of the sulphonic group ($-SO_3^-$) with polycation $[Bi_6O_5(OH)_3]^{5+}$. Such a mechanism can be confirmed according to the results of influence of pH on the removal efficiency. At lower pH values, oxygen atoms (Bi–O and Bi–OH) at the polycation $[Bi_6O_5(OH)_3]^{5+}$ are protonated, thereby reducing the electron density around adjacent Bi atoms, which improves the chemical interaction (coordination bond, most likely bidendate bond of sulphonic groups at bismuth atoms) between the bismuth atoms of sorbent and the sulphonic group ($-SO_3^-$) of the RB19. Therefore, BBN-EtOH has the highest sorption capacity at pH ≤ 2.0, because the strength of the coordination bond between the Bi atoms and $-SO_3^-$ weakens with an increase in pH. The highest sorption capacity at pH ≤ 2.0 also occurs due to better electrostatic attraction between dye and sorbent surface. In addition, the small specific surface area indicates that contribution of physical sorption is low, which confirms that chemical and electrostatic interactions are more likely to be the only way of binding RB19 dye onto sorbent surface.

### 3.2.7 Treatment of Real Polluted River Water

In order to examine potential practical use of BBN-EtOH sorbent in real water treatment, the efficiency of RB19 removal from the model solution of polluted river water was investigated. A sample of the Nišava River, which physicochemical characteristics are shown in Table S1, was taken and filtered using a 0.45-μm regenerated cellulose membrane filter. A pollutant, RB19 dye, was added to such a prepared sample of the river water and in this way, the real polluted river water was simulated. Sorption treatment of 600.0 mg $dm^{-3}$ of RB19 was performed at optimum conditions using sorbent dose of 500.0 mg $dm^{-3}$ and at pH 2.0. The results (Fig. 8) show that the removal efficiency in the model solution of real polluted river water was also high. The obtained sorption capacity was smaller than in the model solutions with deionized water, but still the sorption capacity was very high (1059.98 mg $g^{-1}$), higher than above-mentioned materials from the literature. The decrease in sorption capacity of about 20% occurs due to the presence of organic matter in river water, which can saturate active sites of sorbent. The equilibrium was reached very fast (in one minute) as in the experiments with RB19 solution in deionized water, so the sorption process is very fast. Based on the results of above-described experiment, it can be concluded that BBN-EtOH sorbent can be suitable for practical application in treatment of real polluted water.

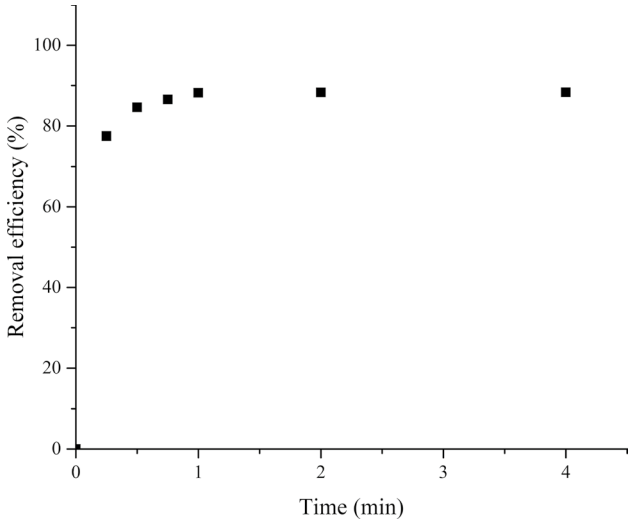


**Fig. 8** Removal efficiency of RB19 from the model solution of real polluted river water; $c_{RB19}$ 600.0 mg dm$^{-3}$, $c_{sorbent}$ 500.0 mg dm$^{-3}$ and temperature 25.0 ± 0.5 °C, pH 2.0

## 4 Conclusions

Pure basic bismuth nitrate $[Bi_6O_5(OH)_3](NO_3)_5{\cdot}2H_2O$ was, for the first time, successfully synthesized by electrochemical deposition from ethanol solution, followed by thermal treatment at 200 °C. The chemical structure of BBN-EtOH was ascertained by XRD, FTIR and EDX analyses. The material is composed of small crystals forming high aggregates. Sorption of RB19 by electrochemically synthesized sorbent (BBN-EtOH) is very fast (above 95% of the total sorption at equilibrium was reached in 1–2 min, depending on the initial concentration of RB19). Sorption kinetics shows that both surface reaction and diffusion were rate-limiting steps. Based on the $r^2$ and MRD, it can be deduced that the experimental data are well fitted by Langmuir, Sips and Brouers–Sotolongo isotherm models. The maximum sorption capacity (1344.99 mg g$^{-1}$) was achieved at pH 2.0. Very high sorption capacity, including treatment in model solution of polluted river water, and fast equilibration are very important characteristics for the potential practical use of BBN-EtOH. Low cost, eco-friendly starting materials, simple and non-time consuming synthesis method, high purity and repeatability of the structure of the synthetized material, as well as very high sorption capacity, better sorption performance and lower sorption equilibrium time than similar materials, make BBN-EtOH sorbent a very attractive system for the removal of textile dyes from polluted water.

**Acknowledgements** The authors would like to acknowledge financial support from the Ministry of Education, Science and Technological Development of the Republic of Serbia (Grant No TR34008).

## References

1. Aksu, Z.; Isoglu, I.A.: Use of agricultural waste sugar beet pulp for the removal of Gemazol turquoise blue-G reactive dye from aqueous solution. J. Hazard. Mater. **137**, 418–430 (2006). https://doi.org/10.1016/j.jhazmat.2006.02.019
2. Menkiti, M.C.; Aniagor, C.O.: Parametric studies on descriptive isotherms for the uptake of crystal violet dye from aqueous solution onto lignin-rich adsorbent. Arab. J. Sci. Eng. **43**, 2375–2392 (2018). https://doi.org/10.1007/s13369-017-2789-3
3. Rajeshwar, K.; Osugi, M.E.; Chanmanee, W.; Chenthamarakshan, C.R.; Zanoni, M.V.B.; Kajitvichyanukul, P.; Krishnan-Ayer, R.: Heterogeneous photocatalytic treatment of organic dyes in air and aqueous media. J. Photochem. Photobiol. C Photochem. Rev. **9**, 171–192 (2008). https://doi.org/10.1016/j.jphotochemrev.2008.09.001
4. O'Neill, C.; Hawkes, F.R.; Hawkes, D.L.; Lourenço, N.D.; Pinheiro, H.M.; Delée, W.: Colour in textile effluents—sources, measurement, discharge consents and simulation: a review. J. Chem. Technol. Biotechnol. **74**, 1009–1018 (1999). https://doi.org/10.1002/(SICI)1097-4660(199911)74:11%3c1009:AID-JCTB153%3e3.0.CO;2-N
5. Ghanbari, F.; Moradi, M.: Electrooxidation processes for dye degradation and colored wastewater treatment. In: Gautam, R.K., Chattopadhyaya, M.C. (eds.) Advanced Nanomaterials for Wastewater Remediation Ravindra, pp. 61–108. CRC Press, Boca Raton (2016)
6. Moussavi, G.; Mahmoudi, M.: Removal of azo and anthraquinone reactive dyes from industrial wastewaters using MgO nanoparticles. J. Hazard. Mater. **168**, 806–812 (2009). https://doi.org/10.1016/j.jhazmat.2009.02.097
7. Dalvand, A.; Nabizadeh, R.; Ganjali, M.R.; Khoobi, M.; Nazmara, S.; Mahvi, A.H.: Modeling of Reactive Blue 19 azo dye removal from colored textile wastewater using L-arginine-functionalized $Fe_3O_4$ nanoparticles: optimization, reusability, kinetic and equilibrium studies. J. Magn. Magn. Mater. **404**, 179–189 (2016). https://doi.org/10.1016/j.jmmm.2015.12.040
8. Gök, Ö.; Özcan, A.S.; Özcan, A.: Adsorption behavior of a textile dye of Reactive Blue 19 from aqueous solutions onto modified bentonite. Appl. Surf. Sci. **256**, 5439–5443 (2010). https://doi.org/10.1016/j.apsusc.2009.12.134
9. Khalid, A.; Zubair, M.: Ihsanullah: a comparative study on the adsorption of Eriochrome Black T dye from aqueous solution on graphene and acid-modified graphene. Arab. J. Sci. Eng. **43**, 2167–2179 (2018). https://doi.org/10.1007/s13369-017-2543-x
10. Yang, Y.; Liang, H.; Zhu, N.; Zhao, Y.; Guo, C.; Liu, L.: New type of $[Bi_6O_6(OH)_3](NO_3)_3{\cdot}1.5H_2O$ sheets photocatalyst with high photocatalytic activity on degradation of phenol. Chemosphere **93**, 701–707 (2013). https://doi.org/10.1016/j.chemosphere.2013.06.062
11. Xie, L.; Wang, J.; Hu, Y.; Zheng, Z.; Weng, S.; Liu, P.; Shi, X.; Wang, D.: Template-free microwave-assisted hydrothermal synthesis and photocatalytic performance of $Bi_6O_6(OH)_3(NO_3)_3{\cdot}1.5H_2O$ nanosheets. Mater. Chem. Phys. **136**, 309–312 (2012). https://doi.org/10.1016/j.matchemphys.2012.08.010
12. He, Y.; Zhang, Y.; Huang, H.; Tian, N.; Luo, Y.: Direct hydrolysis preparation for novel bi-based oxysalts photocatalyst $Bi_6O_5(OH)_3(NO_3)_5{\cdot}3H_2O$ with high photocatalytic activity. Inorg. Chem. Commun. **40**, 55–58 (2014). https://doi.org/10.1016/j.inoche.2013.11.030
13. Abdullah, E.A.; Abdullah, A.H.; Zainal, Z.; Hussein, M.Z.; Ban, T.K.: Bismuth basic nitrate as a novel adsorbent for azo dye removal. J. Chem. **9**, 1885–1896 (2012). https://doi.org/10.1155/2012/617050

14. Zhitomirsky, I.: Cathodic electrodeposition of ceramic and organoceramic materials. Fundamental aspects. Adv. Colloid Interface Sci. **97**, 279–317 (2002). https://doi.org/10.1016/S0001-8686(01)00068-9
15. Thiemig, D.; Bund, A.: Influence of ethanol on the electrocodeposition of Ni/$Al_2O_3$ nanocomposite films. Appl. Surf. Sci. **255**, 4164–4170 (2009). https://doi.org/10.1016/j.apsusc.2008.10.114
16. Brunauer, S.; Emmett, P.H.; Teller, E.: Adsorption of gases in multimolecular layers. J. Am. Chem. Soc. **60**, 309–319 (1938). https://doi.org/10.1021/ja01269a023
17. Barrett, E.P.; Joyner, L.G.; Halenda, P.P.: The determination of pore volume and area distributions in porous substances. I. Computations from nitrogen isotherms. J. Am. Chem. Soc. **73**, 373–380 (1951). https://doi.org/10.1021/ja01145a126
18. Mahmood, T.; Saddique, M.T.; Naeem, A.; Westerhoff, P.; Mustafa, S.; Alum, A.: Comparison of different methods for the point of zero charge determination of NiO. Ind. Eng. Chem. Res. **50**, 10017–10023 (2011). https://doi.org/10.1021/ie200271d
19. Lagergren, S.: About the theory of so-called adsorption of soluble substances. K. Sven. Vetenskapsakademiens Handl. **24**, 1–39 (1898)
20. Ho, Y.S.; McKay, G.: Sorption of dye from aqueous solution by peat. Chem. Eng. J. **70**, 115–124 (1998). https://doi.org/10.1016/S1385-8947(98)00076-X
21. Chrastil, J.: Adsorption of direct dyes on cotton: kinetics of dyeing from finite baths based on new information. Text. Res. J. **60**, 413–416 (1990). https://doi.org/10.1177/004051759006000706
22. Weber, W.J.; Morris, J.C.: Kinetics of adsorption on carbon from solution. J. Sanit. Eng. Div. **89**, 31–60 (1963)
23. Chrastil, J.: Determination of the first order consecutive reaction rate constants from final product. Comput. Chem. **12**, 289–292 (1988)
24. Langmuir, I.: The adsorption of gases on plane surfaces of glass, mica and platinum. J. Am. Chem. Soc. **40**, 1361–1403 (1918). https://doi.org/10.1021/ja02242a004
25. Freundlich, H.: Über die adsorption in lösungen. Z. Phys. Chem. **57**, 385–470 (1906)
26. Sips, R.: On the structure of a catalyst surface. J. Chem. Phys. **16**, 490–495 (1948). https://doi.org/10.1063/1.1746922
27. Brouers, F.; Sotolongo, O.; Marquez, F.; Pirard, J.P.: Microporous and heterogeneous surface adsorption isotherms arising from Levy distributions. Physica A **349**, 271–282 (2005). https://doi.org/10.1016/j.physa.2004.10.032
28. Ncibi, M.C.; Altenor, S.; Seffen, M.; Brouers, F.; Gaspard, S.: Modelling single compound adsorption onto porous and non-porous sorbents using a deformed Weibull exponential isotherm. Chem. Eng. J. **145**, 196–202 (2008). https://doi.org/10.1016/j.cej.2008.04.001
29. Williamson, G.; Hall, W.: X-ray line broadening from filed aluminium and wolfram. Acta Metall. **1**, 22–31 (1953). https://doi.org/10.1016/0001-6160(53)90006-6
30. Liu, X.-D.; Masato, H.; Zheng, X.-G.; Tao, W.-J.; Meng, D.-D.; Zhang, S.-L.; Guo, Q.-X.: Trimeric hydrogen bond in geometrically frustrated hydroxyl cobalt halogenides. Chin. Phys. Lett. **28**, 017803 (2011). https://doi.org/10.1088/0256-307X/28/1/017803
31. Ding, Z.; Lu, G.Q.; Greenfield, P.F.: Role of the crystallite phase of $TiO_2$ in heterogeneous photocatalysis for phenol oxidation in water. J. Phys. Chem. B **104**, 4815–4820 (2000). https://doi.org/10.1021/jp993819b
32. Wajima, T.; Umeta, Y.; Narita, S.; Sugawara, K.: Adsorption behavior of fluoride ions using a titanium hydroxide-derived adsorbent. Desalination **249**, 323–330 (2009). https://doi.org/10.1016/j.desal.2009.06.038
33. Ziegler, P.; Grigoraviciute, I.; Gibson, K.; Glaser, J.; Kareiva, A.; Meyer, H.J.: On the characterization of $BiMO_2NO_3$ (M = Pb, Ca, Sr, Ba) materials related with the Sillén X1 structure. J. Solid State Chem. **177**, 3610–3615 (2004). https://doi.org/10.1016/j.jssc.2004.03.027
34. Carnall, W.T.; Siegel, S.; Ferraro, J.R.; Tani, B.; Gebert, E.: A new series of anhydrous double nitrate salts of the lanthanides. Structural and spectral characterization. Inorg. Chem. **12**, 560–564 (1973). https://doi.org/10.1021/ic50121a013
35. Bünzli, J.-C.G.; Moret, E.; Yersin, J.-R.: Vibrational spectra of anhydrous lanthanum, europium, gadolinium and dysprosium nitrates and oxynitrates. Helv. Chim. Acta **61**, 762–771 (1978). https://doi.org/10.1002/hlca.19780610224
36. Irmawati, R.; Nasriah, M.N.N.; Taufiq-Yap, Y.H.; Hamid, S.B.A.: Characterization of bismuth oxide catalysts prepared from bismuth trinitrate pentahydrate: influence of bismuth concentration. Catal. Today **93–95**, 701–709 (2004). https://doi.org/10.1016/j.cattod.2004.06.065
37. Fruth, V.; Popa, M.; Berger, D.; Ionica, C.M.; Jitianu, M.: Phases investigation in the antimony doped $Bi_2O_3$ system. J. Eur. Ceram. Soc. **24**, 1295–1299 (2004). https://doi.org/10.1016/S0955-2219(03)00506-5
38. Ciobanu, G.; Barna, S.; Harja, M.: Kinetic and equilibrium studies on adsorption of Reactive Blue 19 dye from aqueous solutions by nanohydroxyapatite adsorbent. Arch. Environ. Prot. **42**, 3–11 (2016). https://doi.org/10.1515/aep-2016-0014
39. Ayazi, Z.; Khoshhesab, Z.M.; Norouzi, S.: Modeling and optimizing of adsorption removal of Reactive Blue 19 on the magnetite/graphene oxide nanocomposite via response surface methodology. Desalin. Water Treat. **57**, 25301–25316 (2016). https://doi.org/10.1080/19443994.2016.1157705
40. Khoshhesab, Z.M.; Ahmadi, M.: Removal of reactive blue 19 from aqueous solutions using NiO nanoparticles: equilibrium and kinetic studies. Desalin. Water Treat. **57**, 20037–20048 (2015). https://doi.org/10.1080/19443994.2015.1101713
41. Nga, N.K.; Hong, P.T.T.; Lam, T.D.; Huy, T.Q.: A facile synthesis of nanostructured magnesium oxide particles for enhanced adsorption performance in reactive blue 19 removal. J. Colloid Interface Sci. **398**, 210–216 (2013). https://doi.org/10.1016/j.jcis.2013.02.018
42. Nga, N.K.; Chinh, H.D.; Hong, P.T.T.; Huy, T.Q.: Facile preparation of chitosan films for high performance removal of Reactive Blue 19 dye from aqueous solution. J. Polym. Environ. **25**, 146–155 (2016). https://doi.org/10.1007/s10924-016-0792-5
43. Mirmohseni, A.; Dorraji, M.S.S.; Figoli, A.; Tasselli, F.: Chitosan hollow fibers as effective biosorbent toward dye: preparation and modeling. Bioresour. Technol. **121**, 212–220 (2012). https://doi.org/10.1016/j.biortech.2012.06.067
44. Shanehsaz, M.; Seidi, S.; Ghorbani, Y.; Shoja, S.M.R.; Rouhani, S.: Polypyrrole-coated magnetic nanoparticles as an efficient adsorbent for RB19 synthetic textile dye: removal and kinetic study. Spectrochim. Acta Part A Mol. Biomol. Spectrosc. **149**, 481–486 (2015). https://doi.org/10.1016/j.saa.2015.04.114
45. Kostić, M.; Radović, M.; Velinov, N.; Najdanović, S.; Bojić, D.; Hurt, A.; Bojić, A.: Synthesis of mesoporous triple-metal nanosorbent from layered double hydroxide as an efficient new sorbent for removal of dye from water and wastewater. Ecotoxicol. Environ. Saf. **159**, 332–341 (2018). https://doi.org/10.1016/j.ecoenv.2018.05.015
46. Jia, Z.; Li, Z.; Ni, T.; Li, S.: Adsorption of low-cost absorption materials based on biomass (*Cortaderia selloana* flower spikes) for dye removal: kinetics, isotherms and thermodynamic studies. J. Mol. Liq. **229**, 285–292 (2017). https://doi.org/10.1016/j.molliq.2016.12.059
47. Vijayaraghavan, K.; Mao, J.; Yun, Y.S.: Biosorption of methylene blue from aqueous solution using free and polysulfone-immobilized Corynebacterium glutamicum: batch and column studies. Bioresour. Technol. **99**, 2864–2871 (2008). https://doi.org/10.1016/j.biortech.2007.06.008